THE JOURNAL OF PHYSICAL CHEMISTRY LETTERS
A JOURNAL OF THE AMERICAN CHEMICAL SOCIETY

pubs.acs.org/JPCL

Letter

Understanding Mechanisms of Secondary Active Transport by Analyzing the Effects of Mutations and Stoichiometry

Alex Berlaga and Anatoly B. Kolomeisky*

Cite This: *J. Phys. Chem. Lett.* 2022, 13, 5405−5412

Read Online

ACCESS | Metrics & More | Article Recommendations

ABSTRACT: Biological cells frequently exhibit a so-called secondary active transport by moving various species across their membranes. In this mode of transport, an energetically favorable transmembrane gradient of one type of molecule is used to drive another type of molecule in the energetically unfavorable direction against their gradient. Although it is well established that conformational transitions play a critical role in functioning of transporters, the molecular details of underlying mechanisms remain not well understood. Here, we utilize a recently developed theoretical method to understand better the microscopic picture of secondary active transport. Specifically, we evaluate how mutations in different parts of transporters affect their dynamic properties. In addition, we present a possible explanation on existence of different stoichiometries in the secondary active transport. Our theoretical analysis clarifies several important aspects of complex biological transport phenomena.

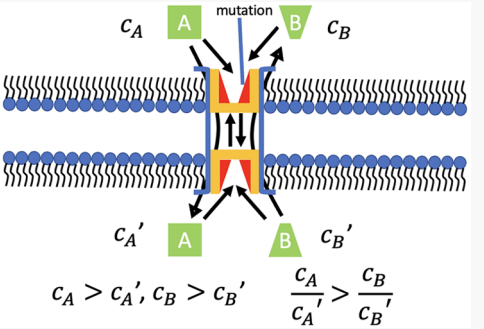

All living systems are built as collections of various organism-specific small compartments that are known as biological cells. These cells are surrounded by membranes that provide an effective protection for processing and regulating the fundamental genetic processes.[1,2] At the same time, the nonequilibrium nature of biological systems requires that some materials be transported in and out of cells by crossing the membranes.[3] For example, this is needed for sending biological signals, for supplying nutrients, and for removal of waste molecules.[3−10] In most cases, this requires an energy input because the involved molecules are large (e.g., sugars, nucleotides, or amino acids), and frequently they must be translocated against their established transmembrane gradients.[3,11]

To support the molecular translocation across the cellular membranes, nature has developed several approaches. One of the most interesting of these approaches is called *secondary active transport* or *cotransport*.[3,11,12] The main idea here is to couple the energetically favorable motion of the first type of molecules to energetically unfavorable motion of the second type of molecules. This is because the first type of molecules, the driving species, would translocate in the direction of their gradient and provide the necessary energy for the second type of molecules, the driven species, to move against their gradient. There are two types of membrane protein channels that support the secondary active transport.[11,13,14] When the direction of fluxes of driving and driven species coincide, the corresponding channels are known as *symporters*, while when the corresponding fluxes are the opposite directions such channels are known as *antiporters*.

The processes associated with secondary active transport in biological cells have been intensively investigated by using a wide spectrum of experimental and theoretical approaches.[8,15−25] It is now well established, both structurally and kinetically, that the molecular transport via antiporters and symporters is taking place via a sequence of conformational transitions that alternate the exposure of the channels to different sides of the cellular membrane.[16,17,24] However, many aspects of the mechanisms of the secondary active transport still remain not well understood. For example, it is still unclear how specific mutations in membrane channels, which is one of the main experimental methods of probing their mechanisms, affect the translocation dynamics and efficiency.[22,26] This is because the analysis of experimentally measured dynamic properties utilizes a purely phenomenological Michaelis−Menten-like approach that has no connection with underlying chemical states. Another interesting question is why different stoichiometries between driving and driven species in the transmembrane transport are frequently observed, even if there is enough energy for the simplest 1:1 stoichiometry to support the translocation.[26,27]

Received: April 25, 2022
Accepted: June 7, 2022
Published: June 9, 2022

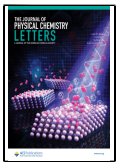

https://doi.org/10.1021/acs.jpclett.2c01232
J. Phys. Chem. Lett. 2022, 13, 5405−5412

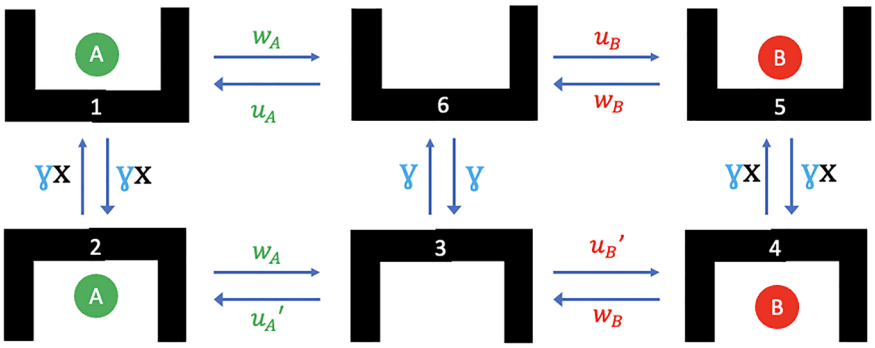

Figure 1. Single-site alternating access model of membrane transport for antiporters with different colors representing the different parameters that might be affected by specific mutations. Green color corresponds to mutations affecting the binding site of molecules *A*, red color represents the mutations to the binding site of molecules *B*, blue color represents mutations that affect the conformational transitions, and black color represents the mutations that change the catalytic effect.

We recently introduced a new theoretical framework to investigate the mechanisms of secondary-active transport.[20,21] This is a minimal chemical-kinetic approach that takes into account the most relevant chemical states and transitions, allowing us to obtain explicit expressions for dynamic properties of antiporters and symporters. This method is filling a theoretical gap between the computational models that concentrate on structure changes during the translocation and phenomenological structureless models that are frequently utilized to analyze the experimental data on dynamics. In this paper, we apply this theoretical approach to clarify two issues, namely, (1) what the effect of specific mutations on dynamic properties is and (2) why the secondary active transport explores various molecular stoichiometries during the membrane translocation. While our theoretical arguments are valid for all types of transporters, to be more specific, we concentrate on antiporters.

Let us consider a chemical-kinetic model, presented in Figure 1, that has been successfully applied to describe the molecular translocation processes in antiporters.[20,21] There are two types of molecules in the system. Molecules of type *A* and *B* have their concentrations above the membrane (outside of cell) as c_A and c_B, respectively, and the concentrations of these species below the membrane (inside the cell) are equal to c_A' and c_B', respectively. While there are more molecules of both types above the membrane ($c_A > c_A'$ and $c_B > c_B'$), molecules *A* are driving molecules *B* across the membrane, i.e., $\frac{c_A}{c_A'} > \frac{c_B}{c_B'}$. This means that the motion of molecules *A* from the upper part to the lower part along their concentration gradient (see Figure 1) provides enough energy to move molecules *B* from the lower part to the upper part against their concentration gradient.

In the chemical-kinetic model presented in Figure 1 there are six possible chemical states. The states 1, 6, and 5 correspond to the situation when the channel is open to the outside, while the states 2, 3, and 4 describe the situation when the channel is facing down. The following chemical transitions might happen in the system. Molecules *A* can bind to the open channel facing up (transition 6 → 1) with a rate $u_A = kc_A$, while the dissociation (transition 1 → 6) is taking place with a rate w_A (see Figure 1). If the channel is open to the inside, then the corresponding association/dissociation rates of the molecules *A* (transitions 3 ↔ 2) are equal to $u_A' = kc_A'$ and w_A' (assumed to be equal to w_A), respectively. Similar transitions happen for the molecules *B* (Figure 1). They can reversibly bind to the channel facing up (transitions 6 ↔ 5) with the rates $u_B = kc_B$ and w_B, while for the channel facing down the corresponding rates (transitions 3 ↔ 4) are $u_B' = kc_B'$ and w_B' (assumed to be equal to w_B), respectively. The antiporter also exhibits conformational transitions that change the orientation of the channel. The empty channel might invert (transitions 6 ↔ 3) with a rate γ (equal rates in both directions), while the conformational rates for occupied channel (transitions 1 ↔ 2 and 5 ↔ 4) are taking place with a rate γx (Figure 1). Here, the dimensionless parameter x specifies a catalytic effect of modifying the conformational transition rates after the molecular associations of molecules *A* or *B* to the channel.[20,21]

The important advantage of chemical-kinetic model is that all dynamic properties of antiporters can be explicitly evaluated in terms of individual transition rates.[20,21] For example, the stationary flux of driven particles *B* can be written as

$$J_B = \frac{\gamma x w_A w_B}{N}[u_B'(w_A + 2\gamma x + u_A x) - u_B(w_A + 2\gamma x + u_A' x)] \tag{1}$$

where N is a normalization constant given by

$$\begin{aligned} N = {} & w_B(w_B + 2\gamma x)[2u_A(\gamma + u_A')x + u_A w_A(1 + x) \\ & + 2w_A(w_A + 2\gamma x) + u_A'(w_A + 2\gamma x + w_A x))] \\ & + u_B'[2\gamma u_A w_B x^2 + w_A^2(w_B + 2\gamma x + w_B x) + 2w_A x(u_A w_B \\ & + 2\gamma^2 x + \gamma(w_B(1 + x) + u_A x)] \\ & + u_B[2\gamma u_A' w_B x^2 + w_A^2(2\gamma x + 2u_B' x + w_B(1 + x)) \\ & + 2w_A x(u_A' w_B + 2\gamma^2 x + \gamma(w_B + (u_A' + 2u_B' + w_B)x))] \end{aligned} \tag{2}$$

This provides an explicit way to quantitatively analyze the effect of specific mutations on dynamics of molecular translocations in antiporters.

Site-directed mutagenesis is a powerful experimental tool that allows to investigate the mechanisms of biological processes.[1,2] It has been also widely utilized for understanding the mechanisms of secondary active transport.[11,16,27,30] The idea of this method is that mutations locally modify the specific chemical states and transitions. Then measuring the changes in the dynamic properties of membrane channels will reflect the contributions from these states and transitions. Applying this idea to our theoretical model in Figure 1, we notice that single-site mutations might affect four different aspects of the chemical-kinetic scheme. First, mutations might modify the

https://doi.org/10.1021/acs.jpclett.2c01232
J. Phys. Chem. Lett. 2022, 13, 5405−5412

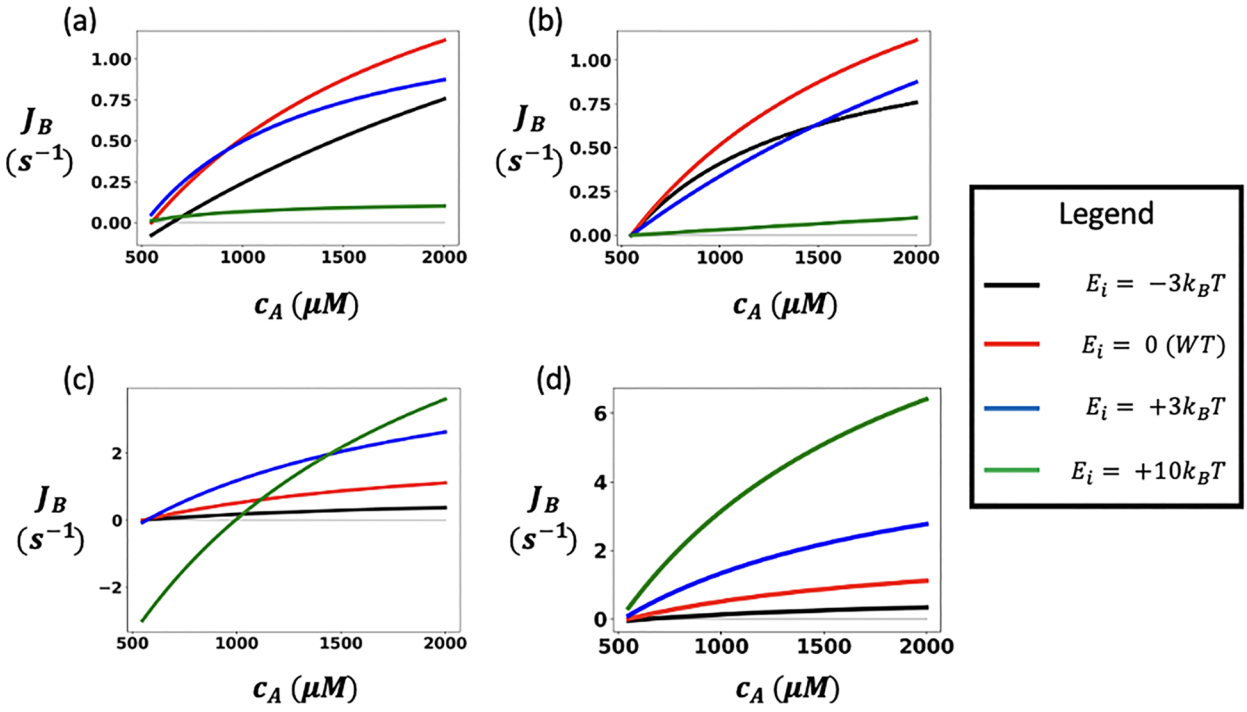

Figure 2. Stationary fluxes of molecules B as a function of the concentration c_A for various mutations: (a) mutations affecting the binding site A; (b) mutations affecting the binding site B; (c) mutations affecting the conformational transitions; and (d) mutations affecting the catalytic effect. In all graphs, the black curves correspond to the energy change scale $E_i = -3\ k_BT$; the red curves correspond to the wild-type systems; the blue curves correspond to the energy change scale $E_i = +3\ k_BT$; and the green curves correspond to the energy change scale $E_i = +10\ k_BT$ with $i = A, B$, *conform*, or *cat*. Also, for calculations the following parameters were utilized: $\gamma(0) = 1\ s^{-1}$, $u_A'(0) = 100\ s^{-1}$, $u_B(0) = 1000\ s^{-1}$, $u_B'(0) = 200\ s^{-1}$, $x(0) = 10$, $w_A(0) = 100\ s^{-1}$, $w_B(0) = 100\ s^{-1}$, and $k = 1\ s^{-1}\ \mu M^{-1}$.

strength of binding of molecules A to protein channel, and the affected transitions rates are shown in green color in Figure 1. Second, mutations might influence the binding of molecules B to the channel, which is shown in red color for the corresponding rates in Figure 1. Third, mutations might change the frequency of conformational transitions, and this is shown in blue color in Figure 1. Finally, mutations might also modify the catalytic effect associated with binding of substrates to the antiporter, and this is illustrated in black color in Figure 1.

To quantify the effect of mutations, we notice that the modifications in the system due to mutations are always associated with some energy changes. Then we can explicitly express the transition rates for the mutated system as a function of the corresponding transition rates for the wild-type system. For mutations affecting the binding of species A, one can write

$$u_A(E_A) = u_A(0)\exp\left(\frac{E_A}{2k_BT}\right);$$
$$u_A'(E_A) = u_A'(0)\exp\left(\frac{E_A}{2k_BT}\right);$$
$$w_A(E_A) = w_A(0)\exp\left(-\frac{E_A}{2k_BT}\right) \quad (3)$$

where E_A is the energy difference in binding molecule A to the antiporter for the mutated system in comparison with the wild-type system; $u_A(0)$, $u_A'(0)$, and $w_A(0)$ are transition rates for the system without mutations. In addition, we assumed here that the energy change due to mutation affects equally the association and dissociation rates, as given by the factor of 1/2 in the exponential terms for each transition rate.

Similarly, if the mutations change the interaction energy between the molecule B and the protein channel by the amount E_B, the corresponding transition rates will be modified as follows:

$$u_B(E_B) = u_B(0)\exp\left(\frac{E_B}{2k_BT}\right);$$
$$u_B'(E_B) = u_B'(0)\exp\left(\frac{E_B}{2k_BT}\right);$$
$$w_B(E_B) = w_B(0)\exp\left(-\frac{E_B}{2k_BT}\right) \quad (4)$$

The mutation can also affect the conformational transition rate that can be expressed as

$$\gamma(E_{conform}) = \gamma(0)\exp\left(\frac{E_{conform}}{k_BT}\right) \quad (5)$$

where $E_{conform}$ is how much the energy barrier for conformational transition changes for the mutated system in comparison with the wild-type system. Similarly, the mutational changes in the catalytic effect can be written as

$$x(E_{cat}) = x(0)\exp\left(\frac{E_{cat}}{k_BT}\right) \quad (6)$$

with E_{cat} being the energy change for this effect.

Associating the effect of mutations with changes in the corresponding energy scales allows us to quantify it, which

https://doi.org/10.1021/acs.jpclett.2c01232
J. Phys. Chem. Lett. 2022, 13, 5405−5412

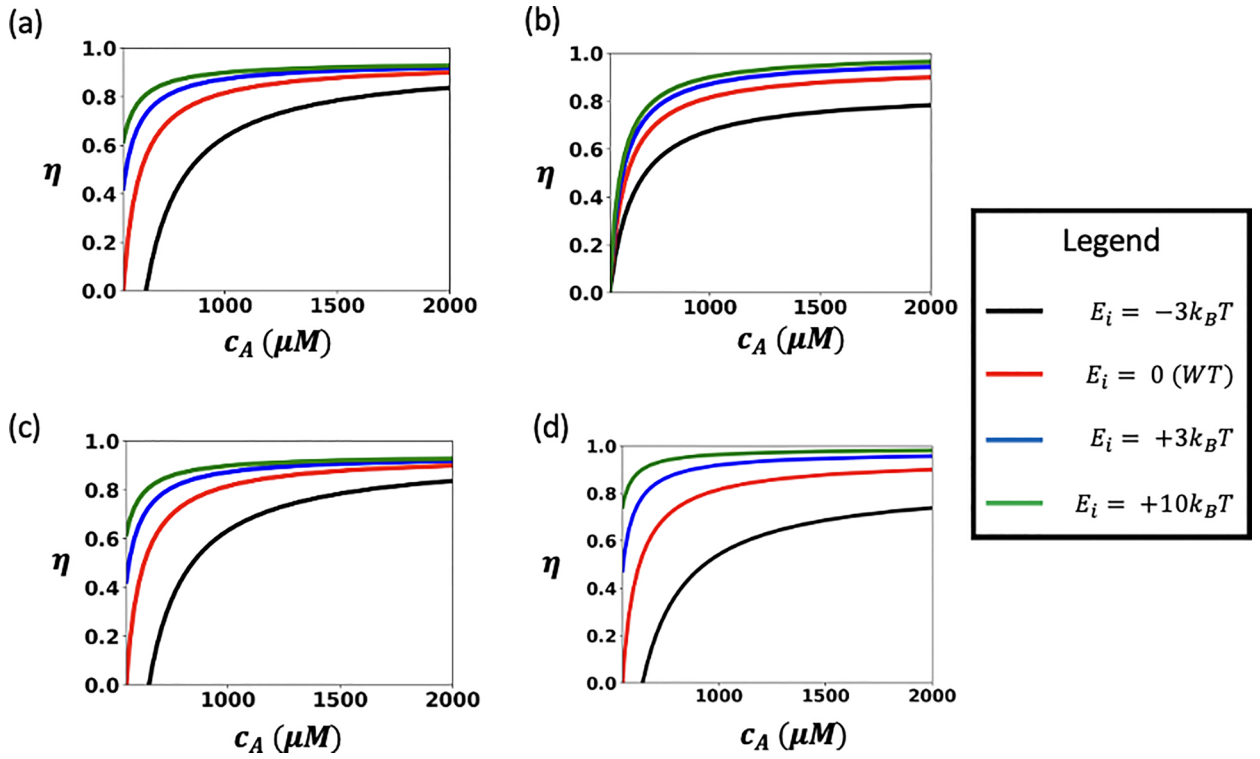

Figure 3. Antiporter efficiency as a function of the concentrations c_A for various mutations: (a) mutations affecting the binding site A; (b) mutations affecting the binding site B; (c) mutations affecting the conformational transitions; and (d) mutations affecting the catalytic effect. In all graphs, the black curves correspond to the energy change scale $E_i = -3\ k_BT$; the red curves correspond to the wild-type systems; the blue curves correspond to the energy change scale $E_i = +3\ k_BT$; and the green curves correspond to the energy change scale $E_i = +10\ k_BT$ with $i = A, B$, *conform*, or *cat*. Also, for calculations the following parameters were utilized: $\gamma(0) = 1\ s^{-1}$, $u_A'(0) = 100\ s^{-1}$, $u_B(0) = 1000\ s^{-1}$, $u_B'(0) = 200\ s^{-1}$, $x(0) = 10$, $w_A(0) = 100\ s^{-1}$, $w_B(0) = 100\ s^{-1}$, and $k = 1\ s^{-1}\ \mu M^{-1}$.

might be also useful for analyzing real experimental data.[26] In Figure 2, we present the results of our explicit calculations for the stationary flux of molecules B, J_B, as a function of varying the concentration of the molecules A above the channel, c_A, for various types of mutations with different mutation strengths.

As one can see in Figure 2a, mutations that increase the binding strength of molecules A to the antiporter (green curve) lower the translocation current. However, weakening the strength of this interaction does not always increase the flux. Our calculations show that there is some range of optimal interaction strengths (red and blue curves) that leads to the maximal flux of molecules B. These observations can be explained by using the kinetic scheme in Figure 1. For strong attractive interactions of molecules A with the channel, the system will be found mostly in states 1 and 2, and this will prevent the flux of molecules B across the membrane. For strong repulsions, the situation is different. In this case, molecules A cannot translocate, and this does not give enough energy to molecules B to move against their gradient (recall that $c_B' < c_B$). The optimal transport can be realized for intermediate values of interaction strengths. One should note that the wild-type system is in this range (red curve).

A similar picture is observed for mutations that affect the interaction strength of molecules B with the antiporter (see Figure 2b). Smaller translocation fluxes of particles B are found for stronger attractions and stronger repulsions, and there is an optimal range of interactions that provide the most efficient translocation. Again, it can be explained by using the chemical-kinetic scheme in Figure 1. For strong attractive interactions, the system is mostly found in states 4 and 5, and this prevents the flux of molecules A, lowering the driving force of the secondary active transport. For strong repulsions, molecules B cannot associate to the channel, and for this reason the transport will not happen. The most optimal conditions correspond to intermediate binding strengths, and the wild-type system is in this range.

Figure 2c illustrates the effect of mutations that modify the conformational transition rates γ. For large concentrations c_A, the increase in the conformational rate improves the flux of molecules B since more particle can move in both directions per unit time. However, for relatively small concentrations c_A, the increase in the rate γ might not be beneficial for driving molecules B because of the stronger effect of the so-called leakage current (transitions 3 → 6 in Figure 1). In this case, the driving force from the translocations of molecules A will be smaller due to the leakage current.[20] At large concentrations c_A, the relative effect of the leakage current is negligible. It is much easier to explain the effect of mutations on the catalytic ability of the antiporter (Figure 2d). As expected, increasing the catalytic effect can only improve in the translocation flux of molecules B.

To understand better the effect of mutations on the secondary active transport, it is convenient to consider an efficiency of membrane channels. It is defined as the ratio of the fluxes for particles B and A, and it is given by[20]

$$\eta = \frac{J_B}{J_A} = \frac{u_B'(w_A + 2\gamma x + u_A x) - u_B(w_A + 2\gamma x + u_A' x)}{u_A(w_B + 2\gamma x + u_B' x) - u_A'(w_B + 2\gamma x + u_B x)} \tag{7}$$

https://doi.org/10.1021/acs.jpclett.2c01232
J. Phys. Chem. Lett. 2022, 13, 5405−5412

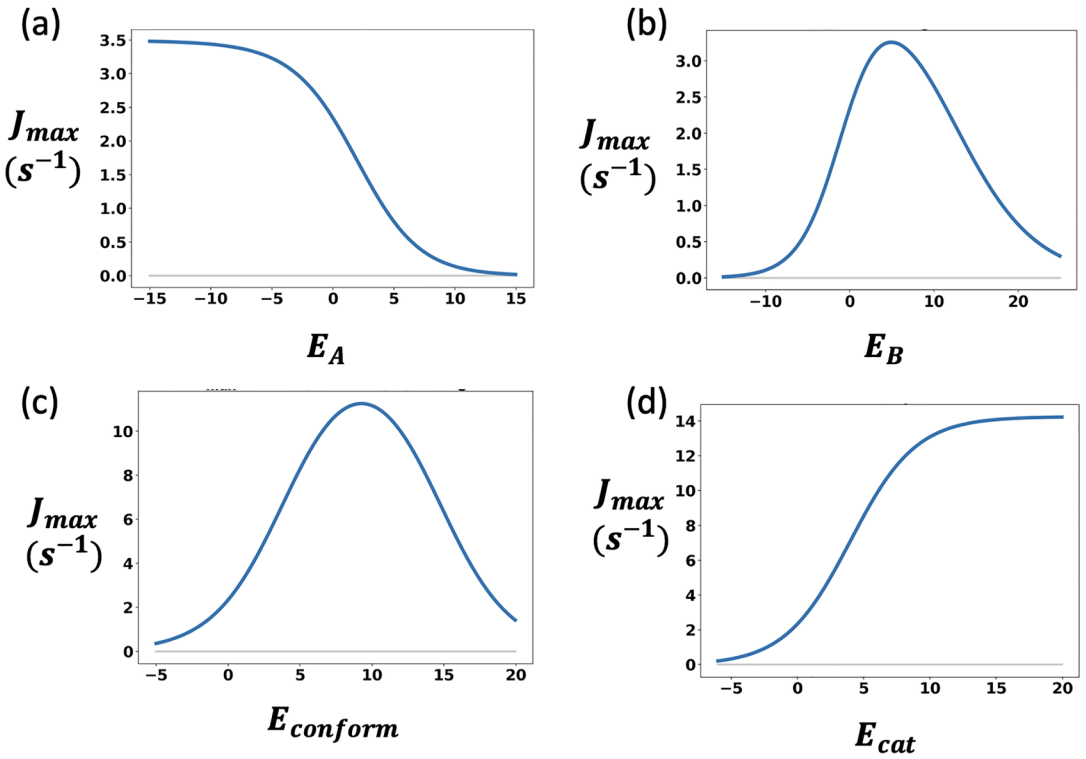

Figure 4. J_{max} as a function of the energy changes (in units of k_BT) due to mutations: (a) mutations affecting binding site A; (b) mutations affecting binding site B; (c) mutations affecting the conformational transitions; and (d) mutations affecting the catalytic effect. For calculations, the following parameters have been used: $\gamma(0) = 1\ s^{-1}$, $u_A(0) = 1000\ s^{-1}$, $u'_A(0) = 100\ s^{-1}$, $u_B(0) = 1000\ s^{-1}$, $u'_B(0) = 200\ s^{-1}$, $x(0) = 10$, $w_A(0) = 100\ s^{-1}$, and $w_B^{(0)} = 100\ s^{-1}$.

This quantity determines how many molecules B can be moved for each translocating molecule A. The results of our calculations for efficiencies are presented in Figure 3. One can see that for any type of mutations increasing the concentration c_A leads to increasing the efficiency, which eventually saturates and reaches $\eta \simeq 1$. For mutations that modify the interaction strength between the molecules A and the channel (Figure 3a), the efficiency is larger for more attractive interactions (green curve). But in this regime only few molecules of A and B are translocated. Similar results are observed for mutations that modify the interactions of the molecules B and the channel (Figure 3b). Also, for mutations that modify the conformational rates (Figure 3c) and the catalytic effect (Figure 3d), increasing the energy scale associated with the corresponding mutations always improves the efficiency.

Comparing the results presented in Figures 2 and 3, we notice that the wild-type antiporters correspond to the intermediate range of energy scales that lead to the maximal possible current of molecules B, but this does not always correspond to the most efficient channels. Thus, we speculate that these protein membrane channels are most probably optimized to obtain the maximal flux of the driven species and not the maximal efficiency. This might be related to the fact that the secondary active transport utilizes already existing concentration gradients of driving species and no additional energy consumption is needed, making the question of increasing the efficiency for biological cells less relevant.

Experimental studies of membrane channels frequently utilize phenomenological Michaelis–Menten-like dependencies of the particles fluxes to probe various aspects of the secondary active transport.[26,27,31] Our theoretical approach is convenient to connect such analysis with more microscopic events that should clarify better the underlying microscopic picture. For this purpose, the molecular flux of molecules B can be written as

$$J_B \simeq \frac{J_{max} c_A}{K_M + c_A} \tag{8}$$

where J_{max} is the maximal possible translocation flux that can be achieved at very large concentrations c_A and K_M is a constant analogous to the Michaelis–Menten constant. It has a physical meaning of concentration c_A at which $J_B = J_{max}/2$. The mechanisms of membrane transport can be understood better by analyzing how different mutations modify the parameters J_{max} and K_M.

It can be shown analytically that

$$J_{\max} = \gamma u'_B w_A w_B x^2 / \{w_B(w_B + 2\gamma x)[(\gamma + u'_A)x + w_A(1 + x)] + 2u'_B x(w_B\gamma x + w_A w_B + w_A\gamma x)\} \tag{9}$$

The effect of different mutations on the maximal current is presented in Figure 4. Mutations that increase the strength of interactions between molecules A and the channel will lead to smaller J_{max}, while the mutations that make these interactions more repulsive will increase the maximal current (see Figure 4a). This can be explained by using the following arguments. For large positive E_A, the channel will be blocked by molecules A, and no translocation for molecules B will happen. The situation is different for large negative E_A. Molecules A should be repelled from the channel, but because the concentration c_A is very large at these conditions, particles A will frequently overcame this repulsion, enter the channel, and translocate, driving the flux of molecules B.

https://doi.org/10.1021/acs.jpclett.2c01232
J. Phys. Chem. Lett. 2022, 13, 5405−5412

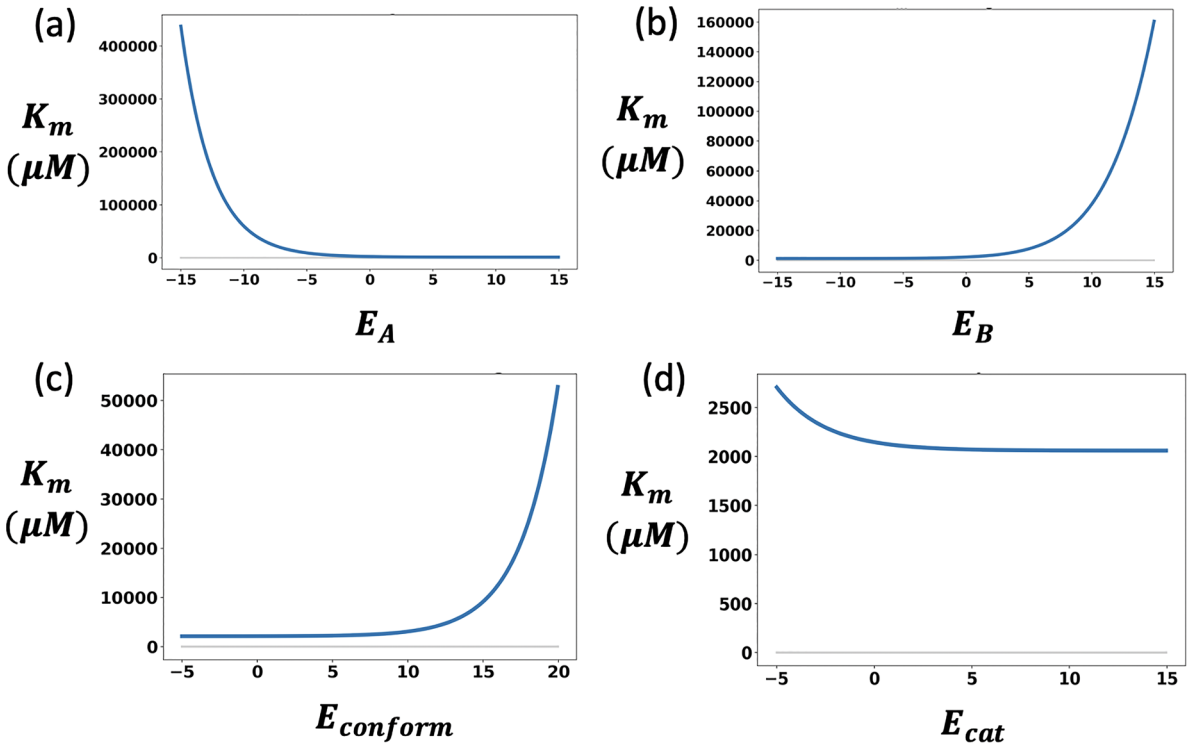

Figure 5. K_M of an antiporter as a function of the energy of its mutation E (in units of k_BT): (a) binding site A mutations, (b) binding site B mutations, (c) conformational change mutations, and (d) catalytic effect mutations. In all curves, $\gamma^{(0)} = 1$, $u_A^{(0)} = 1000$, $u_A'^{(0)} = 100$, $u_B^{(0)} = 1000$, $u_B'^{(0)} = 200$, $X^{(0)} = 10$, $w_A^{(0)} = 100$, and $w_B^{(0)} = 100$.

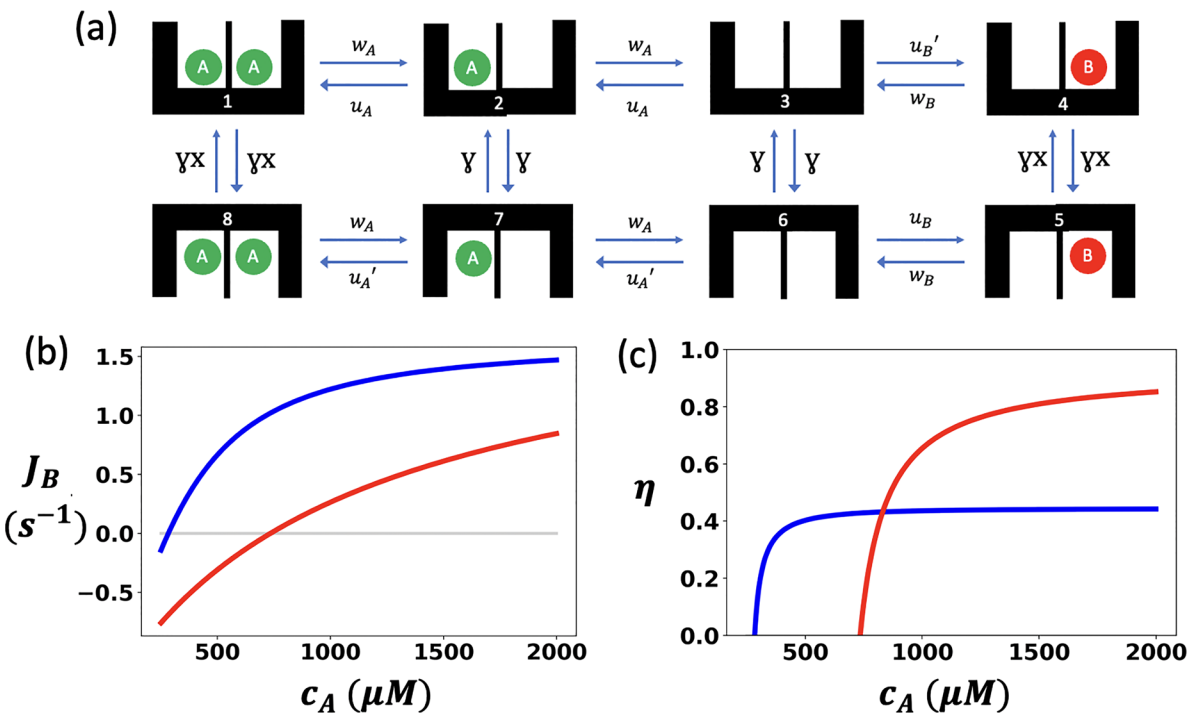

Figure 6. (a) Chemical-kinetic model for antiporter that follows 2:1 stoichiometry. (b) Comparison of stationary particle fluxes for molecules B in the 1:1 stoichiometry model (red curve) and in the 2:1 stoichiometry model (blue curve). (c) Comparison of antiporter efficiencies in the 1:1 stoichiometry model (red curve) and in the 2:1 stoichiometry model (blue curve). The following parameters were used in calculations: $\gamma = 1\ s^{-1}$, $u_A' = 100\ s^{-1}$, $u_B = 1000\ s^{-1}$, $u_B' = 150\ s^{-1}$, $w_A = 100\ s^{-1}$, $w_B = 100\ s^{-1}$, and $x = 10$.

The dependence of J_{max} on varying the strength of mutations that affect the binding of molecules B (Figure 4b) is nonmonotonic. For strong attractions, the channel will be blocked by molecules B, preventing any flux. For strong repulsions, molecules B will not be able even to enter the channel, again preventing any flux. Only for intermediate values of E_B will the particle fluxes of molecules B be observed.

https://doi.org/10.1021/acs.jpclett.2c01232
J. Phys. Chem. Lett. 2022, 13, 5405−5412

A similar nonmonotonic dependence of J_{max} is found for mutations that influence the conformational transitions (Figure 4c). For large negative $E_{conform}$ the conformational transitions will not happen at all, while for large positive $E_{conform}$ the contribution of the leakage current (transitions 3 → 6 in Figure 1) will be too strong for the translocation of molecules A to drive the transport of molecules B. In addition, Figure 4d shows that mutations that increase the catalytic effect will always also increase the maximal possible current for particles B, which is an expected result.

It is also interesting to evaluate the Michaelis−Menten constant in our analytic calculations for different types of mutations. The results are presented in Figure 5. One can see that K_M is strongly affected by mutations in the binding sites for A and B, as well as for the mutations that influence the conformational transitions, while the effect is minimal for those mutations that change the catalytic ability of the antiporter. All trends can be explained by analyzing the chemical-kinetic scheme in Figure 1 and recalling that K_M is a concentration at which the $J_B = J_{max}/2$. For example, K_M decreases with E_A (Figure 5a) because at large attractive interactions the overall fluxes are very small. Then to reach $J_{max}/2$ does not require large values of c_A. At the same time, for strong repulsions the saturating current J_{max} can be reached only for very large concentrations of molecules A, and this also leads to large corresponding K_M. Similar arguments can be presented for other types of mutations.

Our theoretical approach can also be used to answer the question as to why frequently membrane transporters exhibit different stoichiometries despite the fact that from the energetic point of view the simplest 1:1 stoichiometry would be sufficient to drive the molecules across the membrane.[32−34] Our idea is that this might happen when the association of single molecules A does not lead to the strong catalytic effect needed to drive molecules B against their gradient, but having simultaneously several channel-bound molecules A will create the necessary catalytic effect.

To test this hypothesis, we present a chemical-kinetic model for antiporters that can follow 2:1 stoichiometry during the membrane transport, as shown in Figure 6a. In contrast to the original six-state model that describes 1:1 stoichiometry, there are two additional chemical states when the channel is doubly occupied by molecules A (see states 1 and 8 in Figure 6a). We also assume that the single-occupied states (2 and 7) cannot produce the catalytic effect, and the conformational transition rate between them is γ. However, the doubly occupied states (1 and 8) will exhibit the catalytic effect, and the conformational transition rates between them is γx (Figure 6a).

We can explicitly calculate all dynamic properties for the eight-state kinetic model of the antiporter with 2:1 stoichiometry,[20,21] and the results are presented in Figure 6b,c. In these figures, we compare the dynamic properties of antiporters that follow 1:1 stoichiometry (model in Figure 1) and 2:1 stoichiometry (model in Figure 6a). One can see that the current of molecules B significantly increases (Figure 6b), while the efficiency is mostly lower for the 2:1 stoichiometry antiporters (Figure 6c). These observations can be explained by noting that adding two more additional chemical states (Figure 6a) creates a new pathway for molecules A to translocate, and this clearly increases the driving force for molecules B to be moved against their gradient. At the same time, it lowers the efficiency since for one has to double the number of driving species A to achieve the transportation of molecules B. On the basis of these arguments, we speculate that antiporters might follow stoichiometries that deviate from 1:1 if a stronger driving force to move molecules B is needed. This can be accomplished for large concentrations of molecules A (and large gradient $c_A/c'_A \gg 1$), but it will also lead to lower overall efficiency of the antiporter.

In this paper, we presented a theoretical investigation on the effect of mutations in membrane channel proteins that support the secondary active transport. By utilizing a minimal chemical-kinetic model that allows us to obtain explicit expressions for all dynamic properties, we concentrated on antiporters, in which the fluxes of driving and driven species move in opposite directions. In our theoretical analysis, the effect of mutations is associated with changes in energy scales for different chemical transitions. This approach provides a comprehensive quantitative picture of how mutations would modify the properties of antiporters. It is found that there are optimal ranges of mutation effects that lead to largest possible translocation fluxes. We also argue that wild-type membrane protein channels most probably are optimized to obtain the highest fluxes and not to achieve the most efficient performance. In addition, we presented theoretical predictions on how phenomenological parameters that can be obtained from the Michaelis−Menten-like analysis of experimental data will change for different types of mutations. Furthermore, the origin of the existence of antiporters with stoichiometry that deviates from the simplest 1:1 case has been investigated by extending the original chemical-kinetic model. We tested a hypothesis that such deviations might happen when a stronger catalytic effect is needed to drive molecules B against their gradient. It is shown explicitly that the 2:1 stoichiometry model leads to larger particle fluxes and weaker efficiency in comparison with the simplest 1:1 stoichiometry model. The possible conditions that would support more complex stoichiometries are discussed.

Although the presented theoretical study provides a reasonable physical picture of complex processes that are taking place during the secondary active transport in biological cells, it is important to discuss its limitations and shortcomings. To simplify our calculations, several assumptions have been made that might not be always realistic. For example, we assumed that the catalytic effects, expressed by the parameter x, are the same for the molecules of both types, while this might not be the case. In addition, for mutations that change the binding affinities of the substrates with the protein channel it was assumed that the corresponding energy changes affect equally association and dissociation rates. The underlying free-energy landscape associated with such mutations might be more complex, but we expect that this still will not change the main conclusions of our study. It is also important to note that our theoretical analysis has been performed only for antiporters. But it is known that although symporters and antiporters share many similar properties, there are some differences in the mechanisms of translocation adopted by these membrane channels.[20] It will be interesting to explore all these possibilities in more advanced theoretical studies, and it will be also critical to test the obtained theoretical predictions in experimental studies.

AUTHOR INFORMATION

Corresponding Author

Anatoly B. Kolomeisky − *Department of Chemistry, Center for Theoretical Biological Physics, Department of Chemical*

https://doi.org/10.1021/acs.jpclett.2c01232
J. Phys. Chem. Lett. 2022, 13, 5405−5412

and Biomolecular Engineering, and Department of Physics and Astronomy, Rice University, Houston, Texas 77005, United States; orcid.org/0000-0001-5677-6690; Email: tolya@rice.edu

Author

Alex Berlaga − *Department of Chemistry, Rice University, Houston, Texas 77005, United States*

Complete contact information is available at: https://pubs.acs.org/10.1021/acs.jpclett.2c01232

Notes

The authors declare no competing financial interest.

■ ACKNOWLEDGMENTS

This work was supported by the Welch Foundation (C-1559), by the NSF (CHE-1953453 and MCB-1941106), and by the Center for Theoretical Biological Physics sponsored by the NSF (PHY-2019745).

■ REFERENCES

(1) Alberts, B.; Johnson, A.; Lewis, J.; Morgan, D.; Raff, M.; Roberts, K.; Walter, P. *Molecular Biology of the Cell*, 6th ed.; Garland Science: New York, 2014.
(2) Lodish, H.; Zipursky, S. L. Molecular cell biology. *Biochem. Mol. Biol. Educ.* **2001**, *29*, 580−602.
(3) Stillwell, W. *An Introduction to Biological Membranes: Composition, Structure and Function*; Elsevier: 2016.
(4) Stillwell, W. Membrane transport. *An introduction to biological membranes* **2013**, 305.
(5) Faham, S.; Watanabe, A.; Besserer, G. M.; Cascio, D.; Specht, A.; Hirayama, B. A.; Wright, E. M.; Abramson, J. The crystal structure of a sodium galactose transporter reveals mechanistic insights into Na +/sugar symport. *Science* **2008**, *321*, 810−814.
(6) Schulz, A.; Beyhl, D.; Marten, I.; Wormit, A.; Neuhaus, E.; Poschet, G.; Büttner, M.; Schneider, S.; Sauer, N.; Hedrich, R. Proton-driven sucrose symport and antiport are provided by the vacuolar transporters SUC4 and TMT1/2. *Plant Journal* **2011**, *68*, 129−136.
(7) Yang, N. J.; Hinner, M. J. Getting across the cell membrane: an overview for small molecules, peptides, and proteins. *Site-specific protein labeling* **2015**, *1266*, 29−53.
(8) Law, C. J.; Maloney, P. C.; Wang, D.-N. Ins and Outs of Major Facilitator Superfamily Antiporters. *Annu. Rev. Microbiol.* **2008**, *62*, 289−305.
(9) Mueckler, M.; Thorens, B. The SLC2 (GLUT) family of membrane transporters. *Molecular Aspects of Medicine* **2013**, *34*, 121−138. The ABCs of membrane transporters in health and disease (SLC series).
(10) Blaesse, P.; Airaksinen, M. S.; Rivera, C.; Kaila, K. Cation-Chloride Cotransporters and Neuronal Function. *Neuron* **2009**, *61*, 820−838.
(11) LeVine, M. V.; Cuendet, M. A.; Khelashvili, G.; Weinstein, H. Allosteric Mechanisms of Molecular Machines at the Membrane: Transport by Sodium-Coupled Symporters. *Chem. Rev.* **2016**, *116*, 6552−6587.
(12) Poulsen, S. B.; Fenton, R. A.; Rieg, T. Sodium-glucose cotransport. *Current opinion in nephrology and hypertension* **2015**, *24*, 463.
(13) Darrouzet, E.; Lindenthal, S.; Marcellin, D.; Pellequer, J.-L.; Pourcher, T. The sodium/iodide symporter: state of the art of its molecular characterization. *Biochimica et Biophysica Acta (BBA)-Biomembranes* **2014**, *1838*, 244−253.
(14) Navratna, V.; Gouaux, E. Insights into the mechanism and pharmacology of neurotransmitter sodium symporters. *Curr. Opin. Struct. Biol.* **2019**, *54*, 161−170.
(15) Forrest, L. R.; Krämer, R.; Ziegler, C. The structural basis of secondary active transport mechanisms. *Biochimica et Biophysica Acta (BBA)-Bioenergetics* **2011**, *1807*, 167−188.
(16) Boudker, O.; Verdon, G. Structural perspectives on secondary active transporters. *Trends in pharmacological sciences* **2010**, *31*, 418−426.
(17) Shi, Y. Common folds and transport mechanisms of secondary active transporters. *Annual review of biophysics* **2013**, *42*, 51−72.
(18) George, A.; Bisignano, P.; Rosenberg, J. M.; Grabe, M.; Zuckerman, D. M. A systems-biology approach to molecular machines: Exploration of alternative transporter mechanisms. *PLoS computational biology* **2020**, *16*, e1007884.
(19) Bisignano, P.; Lee, M. A.; George, A.; Zuckerman, D. M.; Grabe, M.; Rosenberg, J. M. A kinetic mechanism for enhanced selectivity of membrane transport. *PLoS computational biology* **2020**, *16*, e1007789.
(20) Berlaga, A.; Kolomeisky, A. B. Molecular Mechanisms of Active Transport in Antiporters: Kinetic Constraints and Efficiency. The. *J. Phys. Chem. Lett.* **2021**, *12*, 9588−9594.
(21) Berlaga, A.; Kolomeisky, A. B. Theoretical study of active secondary transport: Unexpected differences in molecular mechanisms for antiporters and symporters. *J. Chem. Phys.* **2022**, *156*, 085102.
(22) Law, C. J.; Yang, Q.; Soudant, C.; Maloney, P. C.; Wang, D.-N. Kinetic Evidence Is Consistent with the Rocker-Switch Mechanism of Membrane Transport by GlpT. *Biochemistry* **2007**, *46*, 12190−12197.
(23) Pradhan, R. K.; Beard, D. A.; Dash, R. K. A biophysically based mathematical model for the kinetics of mitochondrial Na+-Ca2+ antiporter. *Biophys. J.* **2010**, *98*, 218−230.
(24) Drew, D.; Boudker, O. Shared molecular mechanisms of membrane transporters. *Annual review of biochemistry* **2016**, *85*, 543−572.
(25) Bisha, I.; Magistrato, A. The molecular mechanism of secondary sodium symporters elucidated through the lens of the computational microscope. *RSC Adv.* **2016**, *6*, 9522−9540.
(26) Paroder-Belenitsky, M.; Maestas, M. J.; Dohán, O.; Nicola, J. P.; Reyna-Neyra, A.; Follenzi, A.; Dadachova, E.; Eskandari, S.; Amzel, L. M.; Carrasco, N. Mechanism of anion selectivity and stoichiometry of the Na+/I-symporter (NIS). *Proc. Natl. Acad. Sci. U. S. A.* **2011**, *108*, 17933−17938.
(27) Eskandari, S.; Loo, D. D.; Dai, G.; Levy, O.; Wright, E. M.; Carrasco, N. Thyroid Na+/I- symporter: mechanism, stoichiometry, and specificity. *J. Biol. Chem.* **1997**, *272*, 27230−27238.
(28) Turner, R. J. Stoichiometry of Cotransport Systems a. *Ann. N. Y. Acad. Sci.* **1985**, *456*, 10−25.
(29) Johnson, E. A.; Tanford, C.; Reynolds, J. A. Variable stoichiometry in active ion transport: theoretical analysis of physiological consequences. *Proc. Natl. Acad. Sci. U. S. A.* **1985**, *82*, 5352−5356.
(30) Mager, T.; Braner, M.; Kubsch, B.; Hatahet, L.; Alkoby, D.; Rimon, A.; Padan, E.; Fendler, K. Differential Effects of Mutations on the Transport Properties of the Na+/H+ Antiporter NhaA from Escherichia coli*. *J. Biol. Chem.* **2013**, *288*, 24666−24675.
(31) Law, C. J.; Yang, Q.; Soudant, C.; Maloney, P. C.; Wang, D.-N. Kinetic evidence is consistent with the rocker-switch mechanism of membrane transport by GlpT. *Biochemistry* **2007**, *46*, 12190−12197.
(32) Alhadeff, R.; Warshel, A. Simulating the function of sodium/proton antiporters. *Proc. Natl. Acad. Sci. U. S. A.* **2015**, *112*, 12378−12383.
(33) Shlosman, I.; Marinelli, F.; Faraldo-Gómez, J. D.; Mindell, J. A. The prokaryotic Na+/Ca2+ exchanger NCX_Mj transports Na+ and Ca2+ in a 3:1 stoichiometry. *J. Gen. Physiol.* **2018**, *150*, 51−65.
(34) Pradhan, R. K.; Beard, D. A.; Dash, R. K. A Biophysically Based Mathematical Model for the Kinetics of Mitochondrial Na+-Ca2+ Antiporter. *Biophys. J.* **2010**, *98*, 218−230.